MIT Libraries | DSpace@MIT

MIT Open Access Articles

A B12-dependent radical SAM enzyme involved in oxetanocin A biosynthesis

The MIT Faculty has made this article openly available. ***Please share*** how this access benefits you. Your story matters.

Citation: Bridwell-Rabb, Jennifer et al. "A B12-Dependent Radical SAM Enzyme Involved in Oxetanocin A Biosynthesis." Nature 544, 7650 (March 2017): 322–326 © 2017 Macmillan Publishers Limited, part of Springer Nature

As Published: http://dx.doi.org/10.1038/NATURE21689

Publisher: Springer Nature

Persistent URL: http://hdl.handle.net/1721.1/116346

Version: Author's final manuscript: final author's manuscript post peer review, without publisher's formatting or copy editing

Terms of Use: Article is made available in accordance with the publisher's policy and may be subject to US copyright law. Please refer to the publisher's site for terms of use.

Massachusetts Institute of Technology

Author Manuscript

Author Manuscript

Author Manuscript

Author Manuscript

HHS Public Access

Author manuscript

Nature. Author manuscript; available in PMC 2017 September 27.

Published in final edited form as:

Nature. 2017 April 20; 544(7650): 322–326. doi:10.1038/nature21689.

A B_{12}-dependent radical SAM enzyme involved in Oxetanocin-A biosynthesis

Jennifer Bridwell-Rabb[*,1,2,3], **Aoshu Zhong**[*,4,5], **He G. Sun**[4,5], **Catherine L. Drennan**[‡,1,2,3], and **Hung-wen Liu**[‡,4,5]

[1]Howard Hughes Medical Institute, Massachusetts Institute of Technology, 77 Massachusetts Avenue, Cambridge, Massachusetts 02139, USA

[2]Department of Chemistry, Massachusetts Institute of Technology, 77 Massachusetts Avenue, Cambridge, Massachusetts 02139, USA

[3]Department of Biology, Massachusetts Institute of Technology, 77 Massachusetts Avenue, Cambridge, Massachusetts 02139, USA

[4]Division of Chemical Biology and Medicinal Chemistry, College of Pharmacy, University of Texas, Austin, TX 78712, USA

[5]Department of Chemistry, University of Texas, Austin, TX 78712, USA

Summary

Oxetanocin-A (OXT-A, 1) is a potent antitumor, antiviral, and antibacterial compound. Biosynthesis of OXT-A has been linked to a plasmid-borne, *Bacillus megaterium* gene cluster that contains four genes, *oxsA*, *oxsB*, *oxrA*, and *oxrB.* Here, we show that the *oxsA* and *oxsB* genes are both required for the production of OXT-A. Biochemical analysis of the encoded proteins, a cobalamin (Cbl)-dependent *S*-adenosylmethionine (AdoMet) radical enzyme, OxsB, and an HD-domain phosphohydrolase, OxsA, revealed that OXT-A is derived from 2′-deoxyadenosine phosphate in an OxsB-catalyzed ring contraction reaction initiated by H-atom abstraction from C2′. Hence, OxsB represents the first biochemically characterized non-methylating Cbl-dependent AdoMet radical enzyme. X-ray analysis of OxsB reveals the fold of a Cbl-dependent AdoMet radical enzyme for which there are an estimated 7000 members. Overall, this work provides a framework for understanding the interplay of AdoMet and Cbl cofactors and expands the catalytic repertoire of Cbl-dependent AdoMet radical enzymes.

Users may view, print, copy, and download text and data-mine the content in such documents, for the purposes of academic research, subject always to the full Conditions of use: http://www.nature.com/authors/editorial_policies/license.html#termsReprints and permissions information is available at www.nature.com/reprints.

‡Correspondence should be addressed to C.L.D. (cdrennan@mit.edu) or H.-w.L. (h.w.liu@mail.utexas.edu).
*The authors contributed equally to this work.

Author Contributions: J.B.-R. performed crystallography, A.Z. performed genetic experiments, A.Z., H.G.S. performed biochemical assays. J.B.-R., C.L.D., A.Z., H.G.S., and H.-w.L. designed experiments, analyzed data, and wrote the manuscript.

Structures have been deposited to the Protein Data Bank (5UL2, 5UL3, and 5UL4).

The authors declare no competing financial interests.

Online Content: Methods and additional Extended Data display items are available with the online version of the paper; references unique to these sections appear only in the online paper.

Author Manuscript Author Manuscript Author Manuscript Author Manuscript

Oxetanocin-A (OXT-A, **1**) is a nucleoside analog produced by *Bacillus megaterium* NK84-0128[1]. The phosphorylated forms of OXT-A inhibit cellular and viral DNA polymerases[2] and have shown activity against hepatitis B[3] and herpes simplex viruses[1], among others. The plasmid-borne gene cluster for OXT-A biosynthesis and resistance is located within the *Bgl*II-D fragment[4] and contains four open-reading-frames that encode two HD-domain phosphohydrolases (*oxsA* and *oxrB*), a cobalamin (Cbl)-dependent *S*-adenosylmethionine (AdoMet) radical enzyme (*oxsB*), and a pentapeptide repeat protein (*oxrA*). The simplicity of the cluster suggests that OXT-A may be produced through rearrangement of a purine nucleoside co-opted from a primary metabolic pathway. Since AdoMet radical enzymes catalyze some of the most challenging chemical transformations, OxsB is a likely candidate for catalyzing formation of the eponymous oxetane ring.

AdoMet radical enzymes contain a [4Fe-4S] cluster that, when reduced, cleaves AdoMet and produces a highly reactive 5′-deoxyadenosyl radical (5′-dAdo•)[5]. Cbl-binding proteins, on the other hand, generate 5′-dAdo• through homolytic Co-C bond cleavage of adenosylcobalmin[6] and methylate nucleophilic substrates through heterolytic Co-C bond cleavage of methylcobalamin (MeCbl)[6]. With over 7,000 AdoMet radical enzymes now annotated as Cbl-dependent, these dual cofactor enzymes are emerging as a new superfamily[7–16]. Characterized Cbl-dependent AdoMet radical enzymes catalyze methylation of unactivated C- and P-centers[10,12–14,17–20], but not all reactions attributed to this family involve methylation[21]. Here we describe the first characterization of a non-methylating Cbl-dependent AdoMet radical enzyme and the first structure of a superfamily member.

oxsA, *B* are OXT-A biosynthetic genes

A variety of nucleosides and sugars were tested for competence as substrate(s), however, no turnover was observed with any of the compounds tested (Extended Data Fig. 1). These negative results prompted us to take a genetic approach to determine if other gene products are required for OxsB activity. A non-producing, OXT-A resistant strain, *B. megaterium* NRS 269, and an *E. coli-Bacillus* shuttle vector pMM1522 were used in these experiments (Extended Data Fig. 2a). *B. megaterium* NRS 269 carrying the *Bgl*α-D fragment produces OXT-A (Extended Data Fig. 2b). Deletion of *oxsA* or *oxsB*, however, abolishes OXT-A formation, whereas deletion of *oxrA* and *oxrB* has no effect on OXT-A production (Fig 1a). Notably, both OxsA and OxrB are annotated as HD-domain phosphohydrolases, but the lack of OXT-A production in the *oxsA* deletion experiment indicates OxrB cannot fulfill the functional role of OxsA (Fig 1a). In a separate experiment, *B. megaterium* NRS 269 carrying only *oxsA*, *oxsB*, or the *oxsA*/*oxsB* pair was tested for OXT-A production. Here, OXT-A formation was observed only when both *oxsA* and *oxsB* were present, demonstrating again that *oxsA* and *oxsB* are required for OXT-A biosynthesis (Extended Data Fig. 2c).

To verify the above observation, substrate screening was retried using OxsA and reconstituted OxsB. A new product, P2**,** could be detected in the reaction mixture when 2′-deoxyadenosine-5′-monophosphate (dAMP), or its 5′-diphosphate (dADP) or 5′-triphosphate (dATP) form were employed as substrates (Extended Data Fig. 3a). P2 was characterized using MS and ^{1}H NMR and shown to be the aldehyde form of OXT-A 5′-

Author Manuscript Author Manuscript Author Manuscript Author Manuscript

monophosphate (**2** in Fig. 1b, Extended Data Fig. 3b). Upon treatment with $NaBD_4$, **2** is converted to OXT-A 5′-monophosphate (**3** in Fig. 1b), verified based on co-elution with a chemically synthesized standard of **3** (Extended Data Fig. 3c and 4). These results confirm the requirement of OxsB and OxsA in OXT-A biosynthesis and identify dAMP, dADP and dATP as OXT-A precursors (**1** in Fig. 1b). Approximately 4–10 turnovers of dATP to form **2** are observed in a 12-hr incubation using 20 μM OxsB and 20 μM OxsA (see Methods). The aldehydic group of **2** must be reduced to complete OXT-A (**1**) biosynthesis; indeed, when OxsB/OxsA are assayed in the presence of *B. megaterium* NRS 269 cell extracts or horse liver alcohol dehydrogenase, **1** is produced (Extended Data Fig. 3d,e). OxsA was recently shown to catalyze the sequential hydrolysis of mono-, di-, and tri-phosphorylated OXT-A compounds into OXT-A (**3→1**, Fig. 1d)[22], supporting the ability of the OxsB/OxsA pair to turnover dAMP, dADP and dATP.

Importantly, OxsB has all of the hallmarks of an AdoMet radical enzyme; both AdoMet and reductant are required for product formation (Extended Data Fig. 3a) and 5′-dAdoH is generated (Extended Data Fig. 5a). Additionally, when OxsB is incubated with [2′-$^2H_2$]-2′-dAMP, AdoMet, OxsA and reductant, mono-deuterated 5′-dAdoH is formed (Extended Data Fig. 5b), consistent with AdoMet radical chemistry that initiates with hydrogen atom abstraction from C2′ of dAMP. Additional experiments performed using OxsB, OxsA, and [3′-^{2}H]-2′-dAMP show label retention in OXT-A (Extended Data Fig. 5c), further implicating C2′ as the site of hydrogen atom abstraction. All of these results are consistent with the annotation of OxsB as an AdoMet radical enzyme. Furthermore, product formation requires Cbl (Extended Data Fig. 3a), consistent with Cbl-dependent AdoMet radical chemistry.

A new mode of Cbl binding in OxsB

Structures of apo-OxsB (87 kDa), [4Fe-4S] cluster reconstituted OxsB with aquaCbl bound ($OxsB^{Cbl/[4Fe-4S]}$), and $OxsB^{Cbl/[4Fe-4S]}$ with AdoMet bound ($OxsB^{Cbl/[4Fe-4S]/AdoMet}$) were solved to 2.55-, 1.80-, and 1.85-Å resolution, respectively (Extended Data Table 1). These structures show that OxsB is composed of four modular domains (Fig. 2, Extended Data Fig. 6).

Cbl is bound to domain II, a Rossmann fold, which is similar (r.m.s.d of 3.10 Å for 565 atoms) to the Cbl-binding domain of methionine synthase (MetH) despite sharing only 14% sequence identity. As in MetH[23], Cbl is bound to OxsB with its dimethylbenzimidazole (DMB) base displaced (i.e. “base-off”) from Co (Fig. 3a, Extended Data Fig. 7). However, OxsB does not use the classic “His-on” Cbl binding sequence motif (Asp-X-His-X-X-Gly) defined by the MetH structure from which a His residue on the loop that follows β1 (II-β1 loop) replaces DMB as the lower ligand to Co[23]. In OxsB, the II-β1 loop has no His, is fourteen residues long instead of six, and is flexible, changing conformations between apo and Cbl-bound structures to cap the Cbl-binding site (Fig. 3b, Extended Fig. 8a). The closest protein residue to Co, Asn186, is too far (6.4-Å) to serve as a lower ligand, but does make through water contacts to Co (Fig. 3a). Surprisingly, Asn186 does not map to the position of the His ligand in MetH[23], being found instead on a loop following II-β3 in the sequence Ser184-Asn186. These residues align with the highly conserved MetH residues Ser804-

Author Manuscript Author Manuscript Author Manuscript Author Manuscript

Leu806[23]. This Ser interacts with N3 of DMB in MetH and OxsB, whereas Asn/Leu orients the lower ligand of Cbl either by stacking (Leu/His in MetH)[23] or hydrogen bonding (Asn/H_2O in OxsB) (Extended Data Fig. 7b–e)[23]. A water molecule (or hydroxide ion) also appears to ligate Co on the upper face of the OxsB Cbl (Extended Fig. 6c), generating a hexacoordinate form of the cofactor typically associated with a Co(III)-Cbl oxidation state[24]. This base-off, His-off mode of Cbl-binding is unlikely to be unique to OxsB given that the Cbl-dependent AdoMet radical methylase, TsrM, was reported to also bind Cbl base-off, His-off[19].

Overall, modifications to the Cbl-binding domain of OxsB, including the extended II-β1 loop and the absence of a protein-based ligand to Co, result in a shift of the corrin ring approximately 5-Å from the observed position in MetH and closer to the [4Fe-4S] cluster (Fig. 3b). This position of the OxsB corrin ring is approximately 90° away from the standard orientation of a corrin ring with respect to a TIM barrel; Cbl-enzymes typically position the corrin ring directly on top of the C-terminal end of a barrel in the same position that [4Fe-4S] clusters of AdoMet radical enzymes are found (Fig. 3c,d). Here we have an enzyme that accommodates both cofactors, and we find that the [4Fe-4S] cluster is in the standard position at the top of a partial TIM barrel, whereas Cbl has a novel position (Fig. 3d).

Expanded AdoMet fold accommodates Cbl

Comparison of OxsB with a classic AdoMet radical core fold exemplified by *E. coli* pyruvate-formate lyase activating enzyme (PFL-AE)[25], shows an outward displacement of β-strands and helices such that the partial TIM barrel fold of OxsB is now large enough to accommodate Cbl (Fig. 4a). All previously described motifs for AdoMet and cluster binding[26,27] remain intact, albeit with a few notable variations in both their function and structure. For example, in addition to coordinating the [4Fe-4S] cluster, residues of Cys-rich loop (Pro322, His325, and Lys326 of C[313]DYSRC[318]TFC[321]PRDHK[326]) also make contacts with Cbl (Fig. 3a). His325 and Lys326, in particular, move 8.0- and 8.8-Å, respectively, from their positions in the apo-structure to hydrogen bond to Cbl (Extended Data Fig. 8b, c). Similarly, a residue of the “GGE” AdoMet binding motif (Ala361-Glu363) has taken on an auxiliary role; in addition to providing a backbone carbonyl to hydrogen bond with the amino group of AdoMet, the side-chain of Glu363 also interacts with an acetamide moiety of Cbl, tethering Cbl near the [4Fe-4S] cluster (Fig. 3c, Extended Data 7e). Thus, two classic AdoMet radical motifs serve to hold the [4Fe-4S] cluster, AdoMet and Cbl close to each other in OxsB.

The most substantial variation in an AdoMet radical motif is the replacement of β6 with a long loop. This loop connecting the 3_{10} helix to III-α6* lies approximately where β6 ends in PFL-AE, and like β6 in PFL-AE contributes two hydrogen bonds to the AdoMet adenine ring fulfilling the AdoMet binding function (Fig. 4a, b). AdoMet radical enzyme BtrN[28] also uses a loop replacement for a missing β6, but in this case, the loop follows β5 with no intervening helices. Interestingly, OxsB has higher overall structural homology to PFL-AE than BtrN (DALI server[29]), suggesting loss of β6 may have happened more than once.

Author Manuscript Author Manuscript Author Manuscript Author Manuscript

Domain III concludes with a 25-residue loop that follows III-α6* (Fig. 4a) and serves to partially bury the [4Fe-4S] cluster. Even with this loop, however, the active-site is quite open (Extended Data Fig. 8d–f). We suspect that once substrate binds, a conformational change will close the active-site. A comparison of apo- and holo-OxsB structures reveals the helix bundle domain can swing towards the active-site as occurs in MetH[23,30,31] (Extended Data Fig. 8d).

AdoMet samples different conformations

AdoMet binds to the [4Fe-4S] cluster in two conformations, which differ by a 4.0-Å shift in the position of the AdoMet sulfur atom (Fig. 4c, Extended Data Fig. 9). In one conformation, the "radical-competent conformation", the S atom of AdoMet is 3.0-Å away from the [4Fe-4S] cluster (Fig. 4d), comparable to the average 3.4-Å S to Fe distance seen in other AdoMet radical enzymes that permits reductive cleavage of AdoMet[27]. In the second orientation, AdoMet does not engage with the GGE motif and does not appear competent to perform radical chemistry as the S atom is 6.5-Å away from the cluster (Fig. 4d). Instead, this binding mode places AdoMet approximately where one would expect it to bind to methylate Cbl; the methyl is 5.8-Å from Co (Fig. 4e), a similar distance to that found in the reactivation complex of MetH[32]. As OxsB does not catalyze a methylation reaction, this second AdoMet conformation is unlikely to be catalytically relevant. However, it could represent an orientation sampled to minimize uncoupled AdoMet cleavage. Regardless, these structural data on OxsB show that the active site of a Cbl-dependent AdoMet radical enzyme is designed such that two AdoMet binding modes can be populated, one in which AdoMet is positioned for radical chemistry and one in which the methyl group of AdoMet is close to Co. Indeed, recent studies[19,20] performed on TsrM describe a new mode of AdoMet binding; AdoMet binds close to the [4Fe-4S] cluster, but not with traditional coordination through either the amino or carboxylate moieties.

Although we do not have OxsB structures with substrate bound, structures of other AdoMet radical enzymes show that substrate sits in the lateral opening of the barrel such that the site of hydrogen atom abstraction is 3.7–4.0 Å from the 5′ position of AdoMet[27]. Using the substrate-bound structure of PFL-AE[25] as a guide, we can map the approximate site of hydrogen-atom abstraction to a position in OxsB that is equidistant from the 5′-carbon of AdoMet (the radical-competent orientation) and Co of Cbl (Fig. 4f, Extended Data Fig. 8g). This close juxtaposition of the putative substrate-binding site to both cofactors (3.7-Å in both cases) suggests that a hydrogen-atom abstraction step catalyzed by 5′-dAdo• could be followed by a Cbl-dependent reaction without any movement of the substrate or protein. Thus, OxsB may use two common strategies of radical enzymes: a conformational change seals an open active site prior to radical generation, and an arrangement of cofactors that limits the need for conformational changes once highly reactive radical intermediates are formed.

Proposed mechanisms for OXT-A synthesis

The above structural and biochemical data support the involvement of Cbl-dependent AdoMet radical chemistry in formation of the four-membered ring of OXT-A from

Author Manuscript Author Manuscript Author Manuscript Author Manuscript

phosphorylated forms of deoxyadenosine, thereby taking advantage of prevalent compounds in the cell (Fig. 1d, 5). Based on the deuterium labeling experiments, catalysis is likely initiated via hydrogen atom abstraction from C2′ of dAMP, dADP or dATP by 5′-dAdo•. Rearrangement of the resulting substrate radical (**4**) to the product radical (**6**) may proceed via an intermediate enol radical (**4**→**5**→**6**) (Fig. 5), analogous to the Cbl-dependent mutases[33]. Steps **4**→**6** are expected to be thermodynamically unfavorable due to contraction of a five-membered furanosyl ring to an oxetanyl ring. Coupling of this unfavorable reaction to the favorable OxsA phosphate hydrolysis reaction could shift the equilibrium toward product. Additionally, Cbl could play a role in lowering the activation energy barrier for these steps, either through a direct or indirect coordination of a substrate-bound radical. Steps **6** → **2** require an electron acceptor, and Cbl is one possible acceptor; formation of a Cbl-product radical complex could provide a conduit by which the unpaired electron in **6** is transferred to Cob(II) to form **2** and Cob(I). Subsequent electron transfer from Cob(I) to $[4Fe\text{-}4S]^{2+}$ would reset the redox state of the catalytic center. Alternatively, an external electron acceptor could be involved[34], or $[4Fe\text{-}4S]^{2+}$ could accept the electron from **6** as has been proposed for DesII[35]. Finally, the aldehyde product **2** is converted to **3** by a cellular component, which along with dephosphorylation by OxsA completes OXT-A production.

Discussion

This work confirms that *oxsA* and *oxsB* are the essential OXT-A biosynthetic genes; we show here that OxsB uses AdoMet radical chemistry to catalyze ring contraction of a deoxyadenosine phosphate and recently showed that OxsA catalyzes hydrolysis of the resulting phosphorylated OXT-A compounds[22]. Although we do not know the roles of the remaining two genes located within the OXT-A gene cluster, our genetic experiments confirm that they are not required for OXT-A production. We suspect that *oxrA* and *oxrB* are resistance genes in agreement with their annotation. However, it is interesting to consider why resistance genes are necessary in light of our observation that OxsB requires OxsA for activity. The coupling of the two enzyme activities in itself protects the producing organism from the toxic phosphorylated forms of OXT-A; OxsB does not produce phosphorylated OXT-A unless OxsA can dephosphorylate and render the compound inert. However, OXT-A must be quickly exported before endogenous kinases can re-phosphorylate the compound. We hypothesize that the gene products of *oxrA* and oxrB represent the organism's safety net if export is hindered.

We further demonstrate that OxsB catalysis requires Cbl, although the exact role of Cbl in this nonmethylase is not yet clear. The fact that the apo-OxsB structure is almost identical (0.98 Å r.m.s.d) to holo-OxsB argues against a structural role for Cbl, and the location of Cbl in the OxsB active site is certainly consistent with a catalytic one. The OxsB structure reveals adaptions of both the classic AdoMet radical and Cbl motifs that result in the adjacent positioning of cofactors in the active site. These structural features may have evolved to allow for AdoMet radical-mediated Cbl-methylation, and may have been appropriated to assist in OxsB's complex radical-rearrangement, with Cbl retained to facilitate rearrangement or to accept an electron. The latter possibility would seem to be a mundane use for a cofactor that requires 30 enzymes in its biosynthesis.

Author Manuscript Author Manuscript Author Manuscript Author Manuscript

We still have much to learn about the approximately 7000 enzymes that comprise the Cbl-dependent AdoMet radical enzyme superfamily. Already, with only a handful of these enzymes characterized, an impressive list of functions has emerged, ranging from production of antiviral compounds to bacteriochlorophylls. Outside of this enzyme family, there is no precedent for radical-based methylation, or for any of the functions suggested here for Cbl of OxsB. Thus, regardless of the mechanistic details that emerge, new chemical territory will be charted as we continue to explore this impressive enzyme family.

Extended Data

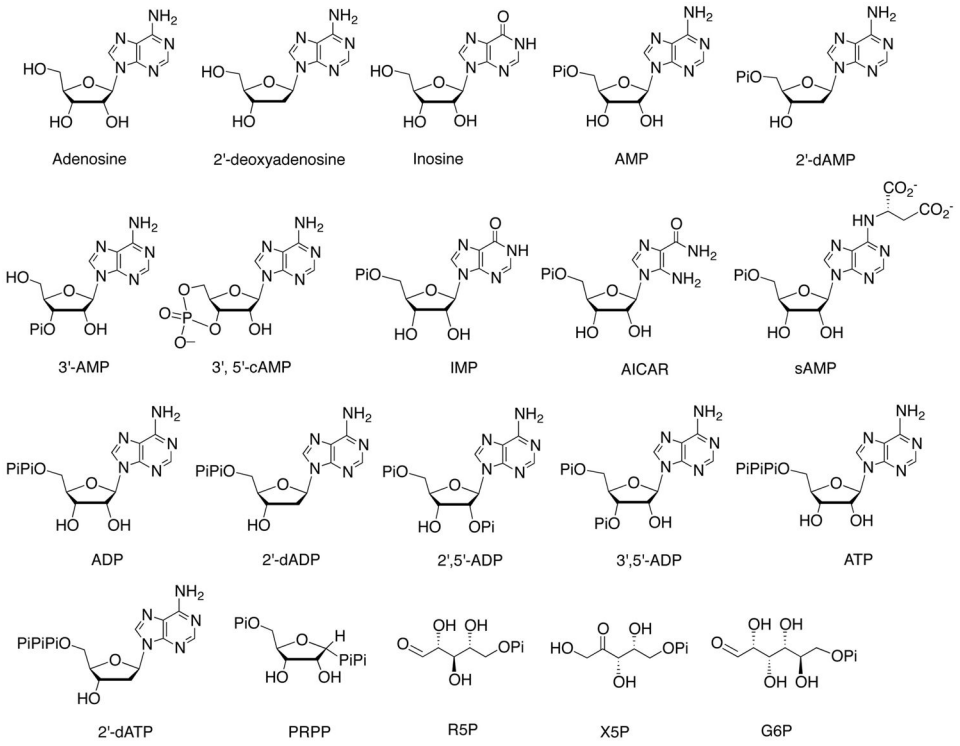

Extended Data Figure 1. Putative substrates tested in the OxsB and OxsA/OxsB reactions

Reductants used to test these substrates were sodium dithionite, hexa-ammineruthenium(II) chloride, NADPH/methylviologen, titanium(III) citrate/methyl viologen, and a flavodoxin/flavodoxin-NADPH reductase system[35,47,48].

Author Manuscript Author Manuscript Author Manuscript Author Manuscript

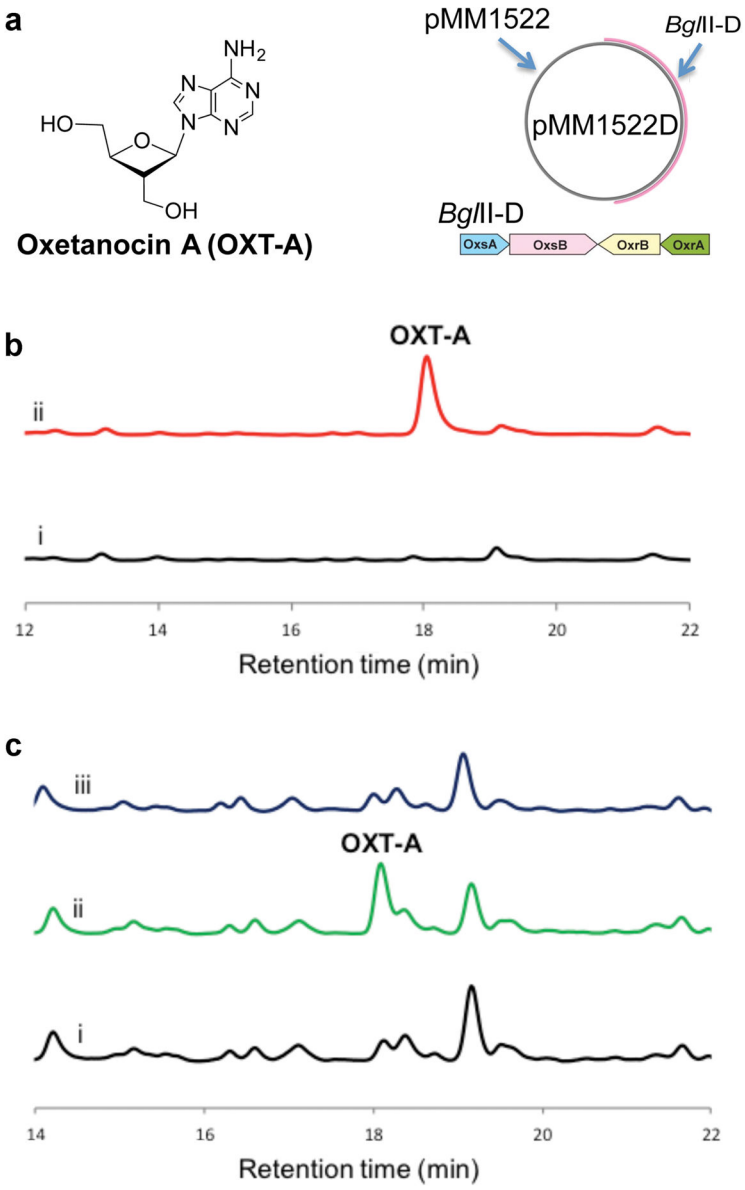

Extended Data Figure 2. In vivo gene expression and HPLC analysis reveal *oxsA* and *oxsB* are required for OXT-A biosynthesis

(a) To probe which genes located within the *Bgl*II-D fragment are responsible for OXT-A (chemical structure shown in left panel) production, *B. megaterium* NRS 269 was transformed using the *E. coli-Bacillus* shuttle vector pMM1522. **(b)** In vivo product profiles of *B. megaterium NRS* 269 strains. (i) transformed with pMM1522 empty vector (as a control); (ii) transformed with pMM1522 that contains the *Bgl*II-D (*oxsA, oxsB, oxrA, oxrB*) fragment. **(c)** In vivo product profiles of *B. megaterium NRS* 269 strains. (i) carrying only *oxsB*; (ii) carrying both *oxsA* and *oxsB*; (iii) carrying only *oxsA*.

Author Manuscript Author Manuscript Author Manuscript Author Manuscript

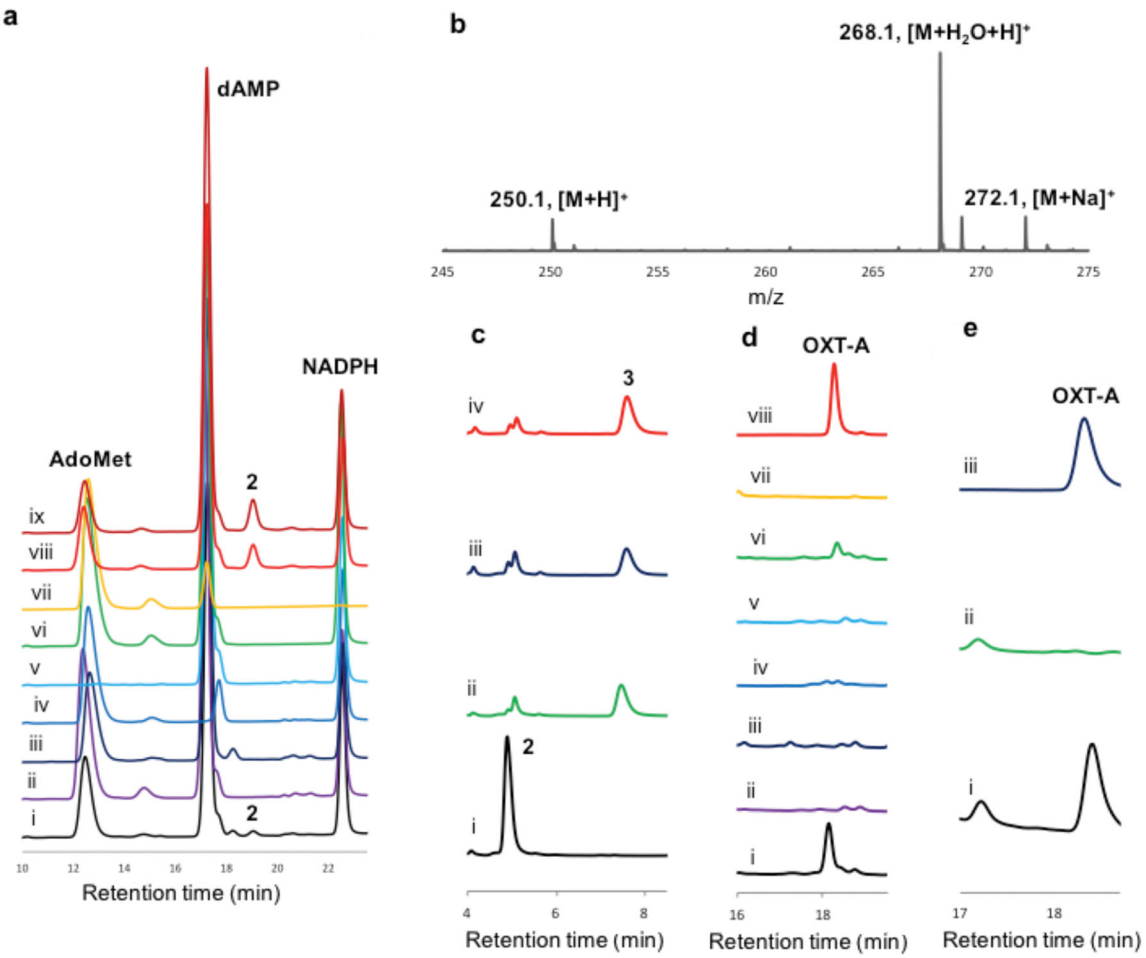

Extended Data Figure 3. Enzymatic production of OXT-A

HPLC analysis in panel a was performed using a CarboPac PA1 Dionex column whereas a C18 column was used in panels c–e. **(a)** HPLC analysis of the reactions catalyzed by OxsA and OxsB using dAMP, dADP, or dATP as substrate. (i) incubation with reconstituted OxsB and OxsA with dAMP, DTT, AdoMet, HO-Cbl, $MgCl_2$, NADPH, MV (full reaction, see Methods for details); (ii) full reaction without OxsB; (iii) full reaction without OxsA; (iv) full reaction without dAMP; (v) full reaction without AdoMet; (vi) full reaction without HO-Cbl; (vii) full reaction without the reductants NADPH and MV; (viii) full reaction substituted with dADP instead of dAMP; (ix) full reaction substituted with dATP instead of dAMP. **(b)** MS spectrum (ESI positive) used to confirm the identity of compound **2** as the corresponding aldehyde of OXT-A 5′-monophosphate. MS of the aldehyde compound was performed following treatment of the reaction mixture with CIP and purification by HPLC. **(c)** HPLC analysis confirms that reduction of compound **2** results in formation of OXT-A-P **(3).** (i) isolated **2**; (ii) isolated **2** treated with $NaBD_4$; (iii) co-injection of **2** treated with $NaBD_4$ with a chemically synthesized standard of **3**; (iv) standard of **3. (d)** Direct formation of OXT-A is observed when cell extract is included in the reaction conditions. (i) HPLC analysis after incubation of reconstituted OxsB with OxsA, dATP, DTT, AdoMet, HO-Cbl, $MgCl_2$, NADPH, MV, and cell extract of *B. megaterium* NRS 269 (full reaction); (ii) full reaction without OxsB; (iii) full reaction without OxsA; (iv) full reaction without dATP; (v)

Author Manuscript Author Manuscript Author Manuscript Author Manuscript

full reaction without AdoMet; (vi) full reaction without $MgCl_2$; (vii) full reaction without cell extract; (viii) OXT-A (**1**) standard. **(e)** Direct formation of OXT-A can also be observed when alcohol dehydrogenase is included in the reaction mixture. (i) HPLC analysis after incubation with reconstituted OxsB and OxsA with dATP, DTT, AdoMet, HO-Cbl, $MgCl_2$, NADPH, MV and horse liver alcohol dehydrogenase (full reaction); (ii) full reaction without OxsA and OxsB; (iii) OXT-A standard.

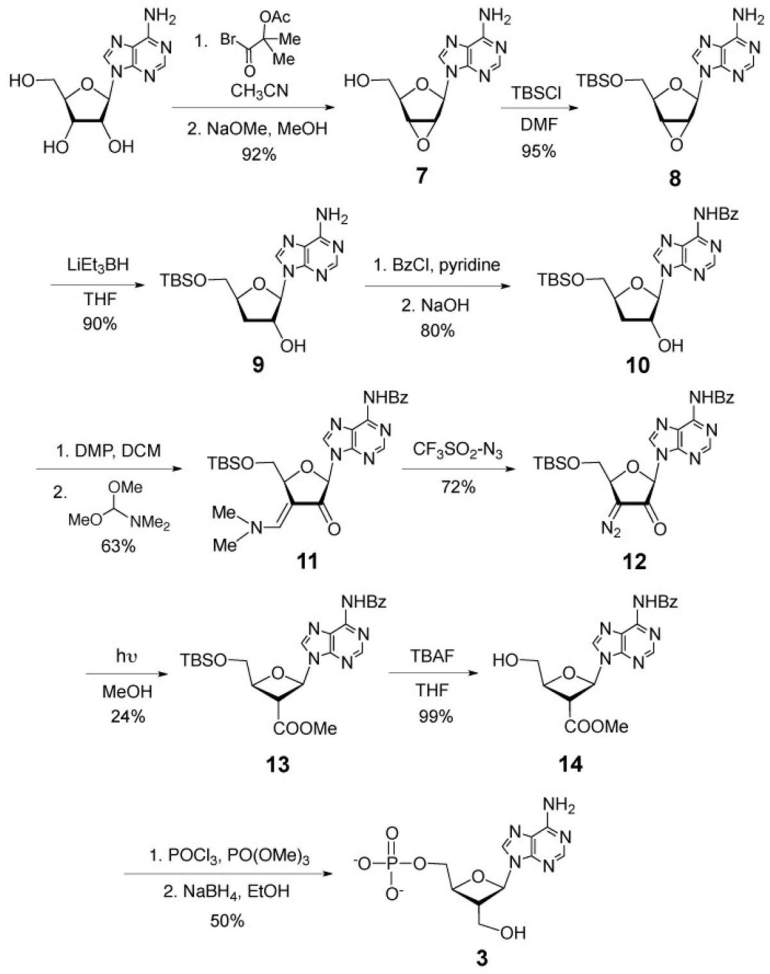

Extended Data Figure 4. Chemical synthesis of OXT-A-P (3)

Author Manuscript Author Manuscript Author Manuscript Author Manuscript

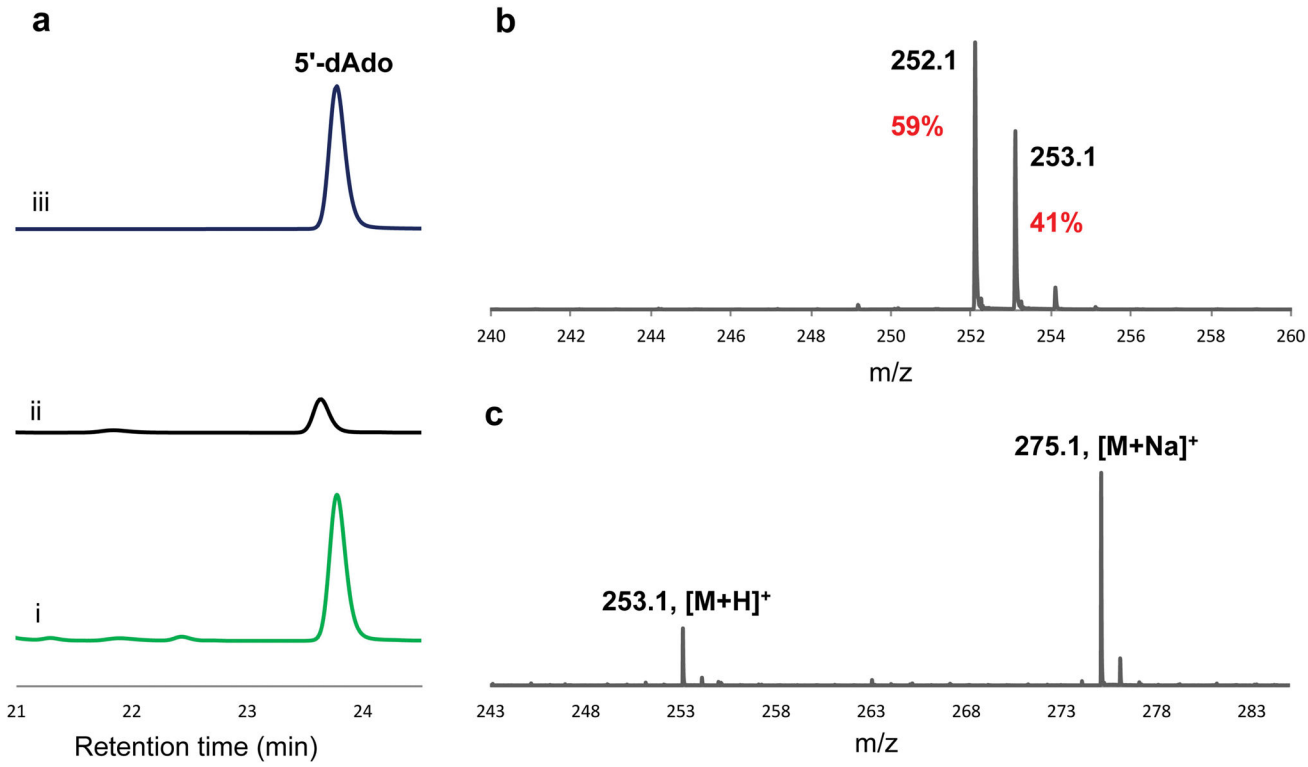

Extended Data Figure 5. Characterization of OxsB as an AdoMet radical enzyme

(a) Consistent with its classification as an AdoMet radical enzyme, OxsB catalyzes the reductive cleavage of AdoMet to generate 5′-dAdoH. HPLC analysis (C18 column, 2–20% CH_3CN in 1% NH_4OAc linear gradient elution) of reaction catalyzed by OxsA and OxsB. (i) Reaction of reconstituted OxsB with OxsA, dAMP, DTT, AdoMet, HO-Cbl, $MgCl_2$, NADPH, MV (full reaction, see Methods for details); (ii) full reaction without dAMP; (iii) 5′-dAdoH standard. **(b)** MS spectrum (ESI positive) of 5′-dAdoH generated in the OxsA and OxsB reaction using [2′-$^2H_2$]-2′-dAMP as substrate shows incorporation of the deuterium label into 5′-dAdoH and thus indicates hydrogen atom abstraction occurs at C2′. The less than full deuterium incorporation is likely due to the co-occurrence of uncoupled quenching of 5′-dAdo•, a common phenomenon in many AdoMet radical enzymes[59]. **(c)** MS spectrum (ESI positive) of OXT-A **(1)** generated in the OxsA and OxsB reaction using [3′-^{2}H]-2′-dAMP as substrate, which shows retention of the deuterium label in product, again consistent with hydrogen atom abstraction at C2′.

Author Manuscript Author Manuscript Author Manuscript Author Manuscript

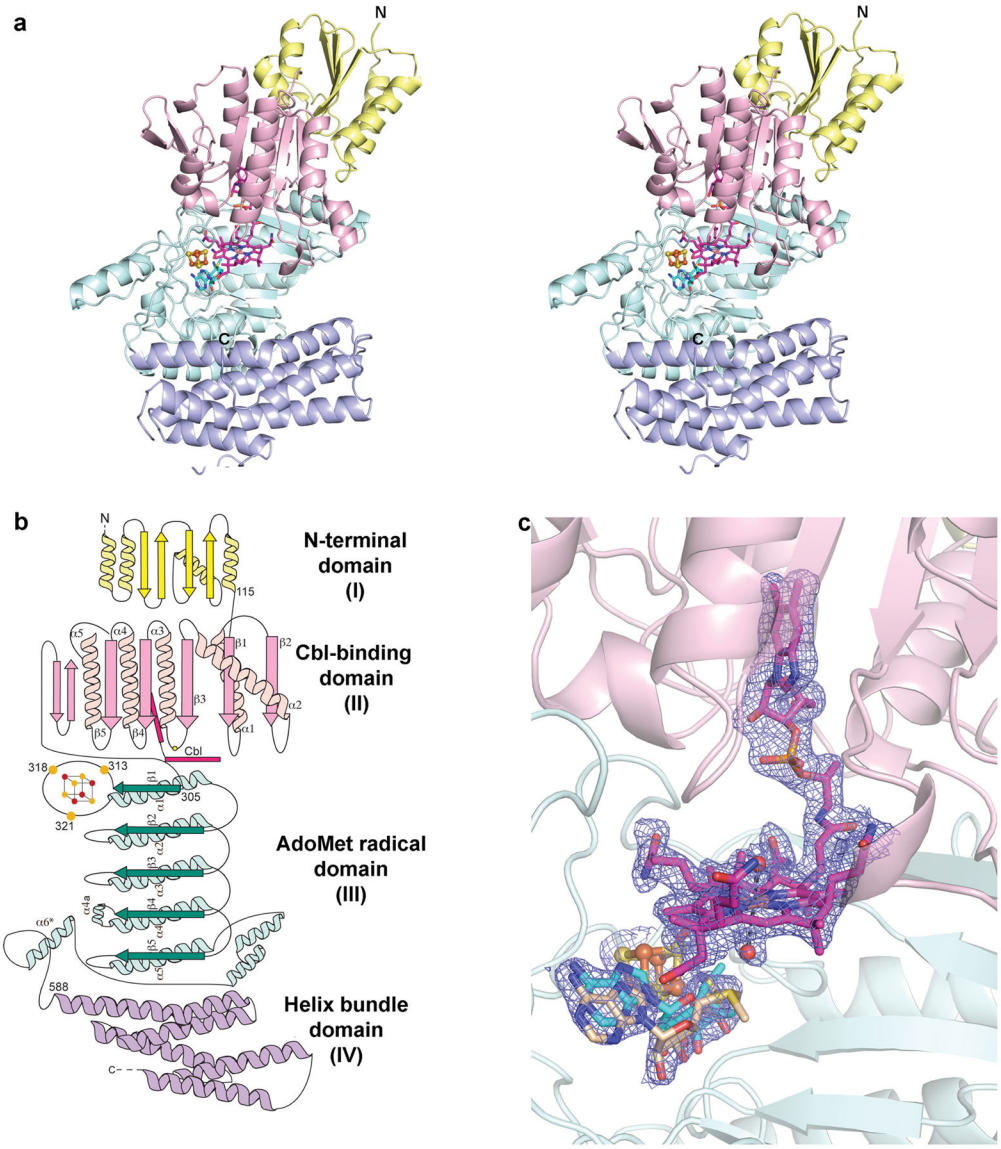

Extended Data Figure 6. OxsB is organized into four modular domains

(a) A stereoview of the entire (744 amino acids) monomer of OxsB colored by domain. The N-terminal domain is shown in yellow, and is followed by the Cbl-binding domain displayed in pink, the AdoMet radical domain, which is colored cyan, and the C-terminal helix bundle domain displayed in blue. **(b)** A topology diagram of OxsB is shown and colored similarly to panel a. The yellow sphere in domain II represents the position of Asn186, which is the closest residue to the Co of Cbl. **(c)** The two observed conformations of AdoMet (cyan and wheat), Cbl, and the [4Fe-4S] AdoMet radical cluster (orange and yellow spheres) are shown with simulated annealing composite omit electron density maps contoured at 0.8 σ.

Author Manuscript Author Manuscript Author Manuscript Author Manuscript

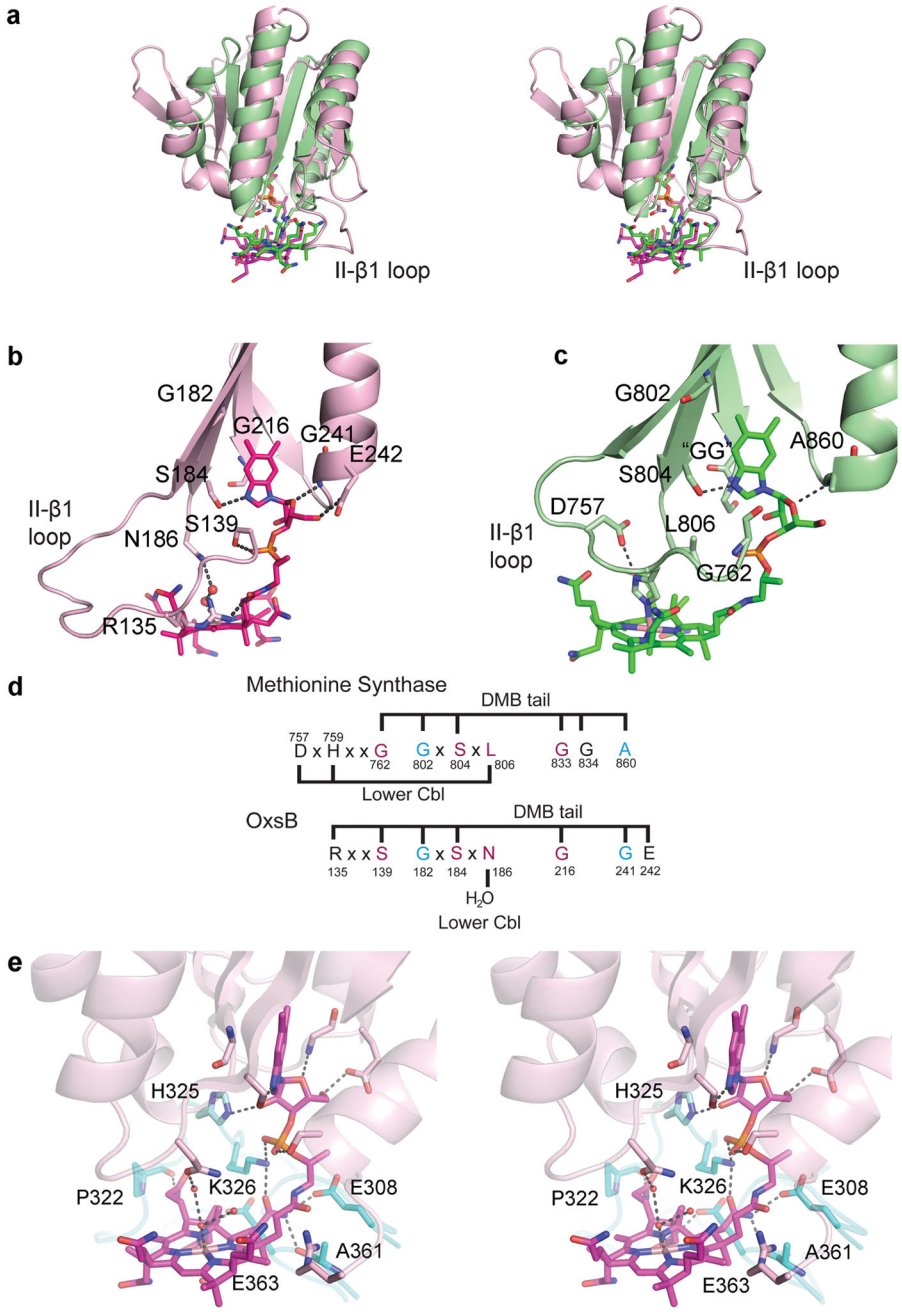

Extended Data Figure 7. Cbl interactions in OxsB and comparison to MetH

(a) A stereoview of an overlay of the MetH[23] Cbl-binding domain (green) with the Cbl-binding domain of OxsB (pink) shows differences in the length of the II-β1 loop, which for OxsB lacks a His residue to ligate Cbl, and the positioning of the Cbl cofactor's corrin ring. **(b)** Residues from the Cbl-binding domain of OxsB that accommodate or make contacts to the DMB tail and corrin ring of Cbl are highlighted and shown as sticks. Residues Gly216 are Ser184 are from the base-off consensus sequence and residues R135–S139 are located on the II-β1 loop. **(c)** Residues from the Cbl-binding domain of MetH[23] that interact with Cbl, or make room for the DMB tail are highlighted and shown as sticks. **(d)** Residues from

Author Manuscript Author Manuscript Author Manuscript Author Manuscript

Figure panels b and c that make contacts to Cbl from the Cbl-binding domains of MetH (top panel) and OxsB (bottom panel) are shown. Residues highlighted in pink are previously identified sequence fingerprints of MetH that have a conserved interaction in OxsB. Residues highlighted in blue are conserved interactions between Cbl and MetH or OxsB, which are not from the standard Cbl-binding motifs. Residues shown in black form interactions with Cbl, but are not conserved between the proteins. **(e)** Stereoview of the contacts that Cbl makes with the Cbl-binding (pink) and AdoMet radical (cyan) domains of OxsB. All of the residues that form interactions with Cbl are highlighted as sticks, but only residues from the AdoMe radical domain are labeled for clarity.

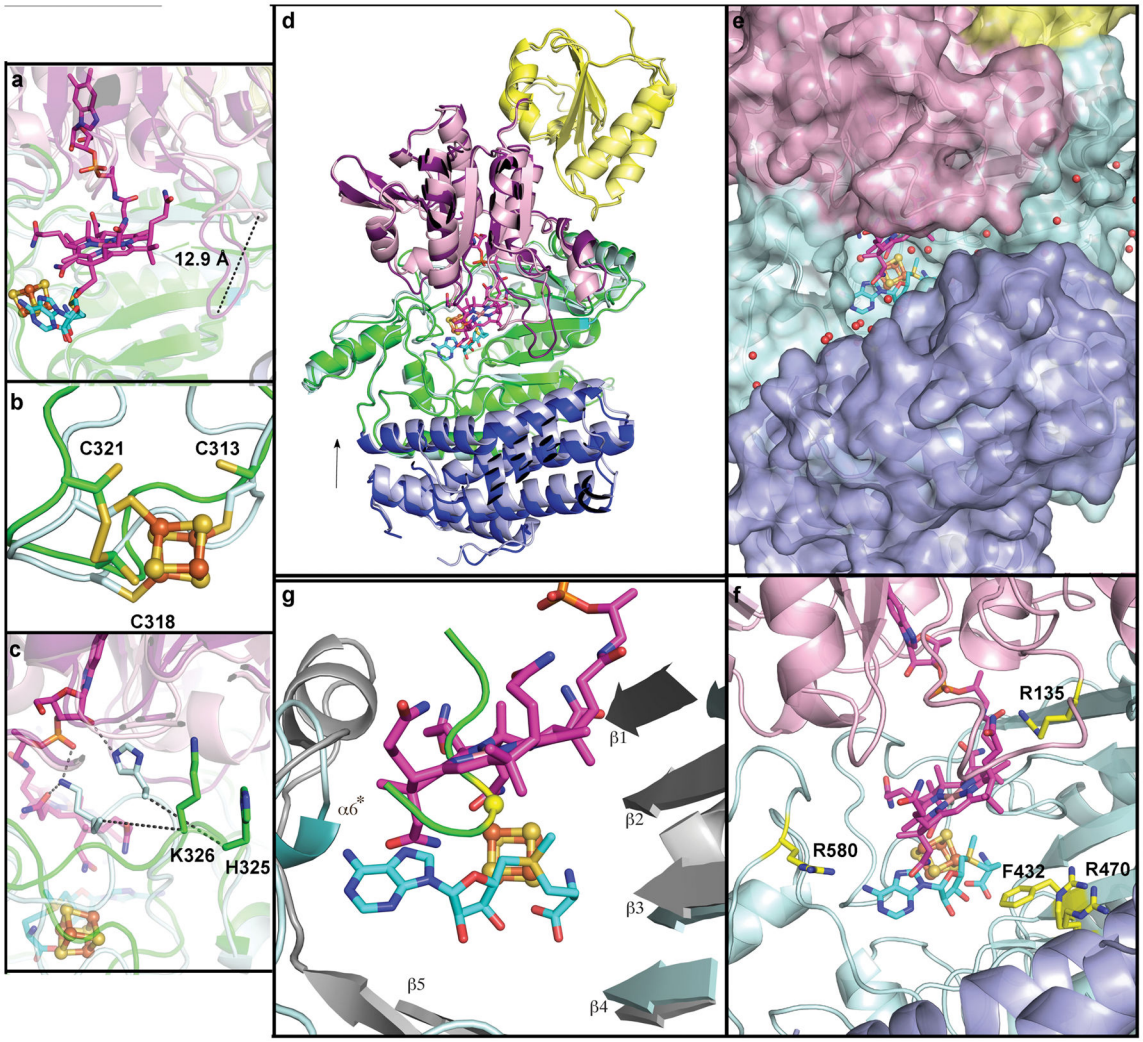

Extended Data Figure 8. Structural comparisons of apo-OxsB, OxsB$^{Cbl/[4Fe-4S]/AdoMet}$, and PFL-AE

(a–d) Small conformational changes occur in the reconstituted structures relative to the apo-structure. The r.m.s.d determined by PyMOL for the OxsB$^{Cbl/[4Fe-4S]/AdoMet}$ structure compared to the apo structure is 0.98 Å for 4770 atoms. **(a)** The II-β1 loop of the Cbl-binding domain in the reconstituted OxsB structures swings outward 12.9-Å to avoid steric

Author Manuscript Author Manuscript Author Manuscript Author Manuscript

clashes with the corrin ring of Cbl and now caps the side of the Cbl. **(b,c)** In the absence of a [4Fe-4S] cluster, the Cys residues of the cluster-binding loop in the apo-structure are oriented similarly to those in the reconstituted structure. Cys318 and Cys321 in the apo-structure, however, exhibit a partial occupancy disulfide linkage. At the end of the cluster binding loop, there are more substantial differences between the structures; His325 and Lys326 of $OxsB^{Cbl/[4Fe\text{-}4S]/AdoMet}$ move 8.0- and 8.8-Å, respectively, from their positions in the apo-structure to interact with the nucleotide tail of Cbl. **(d)** An overlay of $OxsB^{Cbl/[4Fe\text{-}4S]/AdoMet}$ (light colors) with apo-OxsB (dark colors) shows slight movements in each domain. The arrow indicates closing in of the helix bundle domain towards the cofactors. **(e)** A surface representation of OxsB reveals the open and solvent accessible nature of the active site in $OxsB^{Cbl/[4Fe\text{-}4S]/AdoMet}$. Water molecules are shown as red spheres. **(f)** Location of polar and aromatic residues near the active site. Presumably, positively charged residues are needed to accommodate the negatively charged phosphate moieties of substrate and an aromatic residue may stack with substrate adenine. **(g)** An overlay of the β-strands from the AdoMet radical domains of OxsB (cyan) with those from a peptide-bound (green) stucture of PFL-AE[25] (gray) was used to map the approximate substrate binding site in OxsB. The yellow sphere, which corresponds to the Cα of the substrate peptide Gly residue, is 3.7-Å away from the 5′-carbon of AdoMet and 3.7-Å away from Co of Cbl.

Author Manuscript Author Manuscript Author Manuscript Author Manuscript

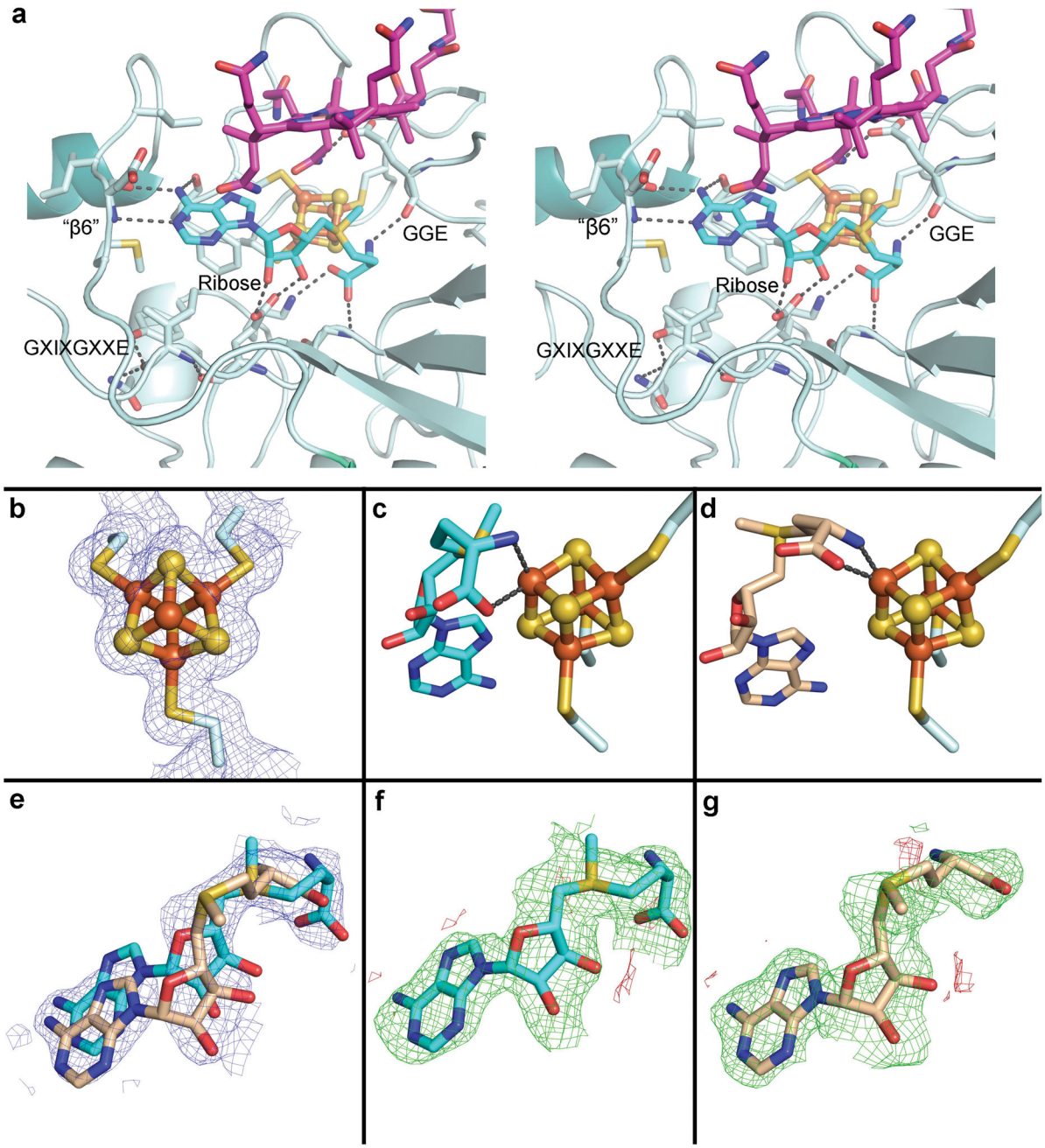

Extended Data Figure 9. AdoMet interactions

(a) A stereoview of the AdoMet radical domain of OxsB. Each of the AdoMet radical motifs[26,27] is highlighted including the GGE (E363), ribose (E436), GXIXGXXE (I474), and the β6 (adenine-binding) motif (E545). The GGE motif provides a carbonyl to hydrogen bond with the amino moiety of AdoMet. In OxsB, E363 also contacts a Cbl acetamide. The ribose motif is found at the C-terminal loop following III-β4 where Glu436 forms two hydrogen bonds with the AdoMet ribose hydroxyl moieties. In the same loop, two residues upstream, the backbone amide of Gly434 contributes a hydrogen bond to the carboxyl group of AdoMet. Following a short III-α4a helix that connects III-β4 and III-α4, Lys448 interacts

Author Manuscript Author Manuscript Author Manuscript Author Manuscript

with the AdoMet carboxylate similar to what was previously observed in QueE[60], HemN[61], HydE[62], PylB[63], anSMEcpe[64], and BtrN[28]. In terms of the GXIXGXXE motif, Ile474 from a loop following III-β5 provides hydrophobic contacts to the adenine ring of AdoMet as observed previously. However, instead of the backbone of Ile474 being stabilized by a polar residue on III-α5, as found in other AdoMet radical enzymes, the backbone of Ile474 is stabilized through interactions with the side chains of Gln442 and Tyr446 from III-α4a and the backbone of ribose motif residue Glu436. The final motif, the so-called β6 motif, is present although β6 is not. A loop substitutes for β6, with backbone atoms of E545 making hydrogen bonds to the adenine ring of AdoMet. Additional residues F320, M544, I546, and L547 that provide hydrophobic interactions to the adenine ring of AdoMet and a hydrogen bond to N6 are also shown. **(b)** A 2F(o)–F(c) simulated annealing composite omit electron density map contoured at 1.0 σ around the AdoMet radical [4Fe-4S] cluster. (**c)** The "radical-competent" orientation of AdoMet ligates the unique Fe of the AdoMet radical [4Fe-4S] cluster, which is shown rotated ~90° from panel b. The distance between the unique Fe and the AdoMet amino and carboxylate moieties measure 2.2 Å each. **(d)** The non-radical competent orientation also ligates the AdoMet radical [4Fe-4S] cluster with the amino and carboxylate moieties. These distances measure 2.3- and 2.0 Å, respectively. **(e)** A 2F(o)–F(c) simulated annealing composite omit electron density map contoured at 1.0 σ around the two orientations of AdoMet. **(f)** A simulated annealing composite omit electron density map calculated after the "radical-competent" orientation of AdoMet was omitted from the refined structure of $OxsB^{Cbl/[4Fe\text{-}4S]/AdoMet}$. This map is contoured at ±3.0 σ around the "radical-competent" orientation of AdoMet. **(g)** A similar simulated annealing composite omit electron density map was calculated after the "non-radical competent" orientation of AdoMet was omitted from the refined structure of $OxsB^{Cbl/[4Fe\text{-}4S]/AdoMet}$. This map is also contoured at ±3.0 σ around the observed AdoMet conformation.

Extended Data Table 1

Data collection and refinement statistics of OxsB

	Apo-OxsB Native data used for SIRAS	SeMet Apo-OxsB†§ (Se-peak, dataset 1)	SeMet Apo-OxsB†§ (Se-peak, dataset 2)	SeMet Apo-OxsB (Se-peak, dataset 3)	OxsB Cbl/[4Fe4S]	OxsB Cbl/[4Fe4S]/AdoMet
Data collection						
Space group	$P2_12_12_1$	$P2_12_12_1$	$P2_12_12_1$	$P2_12_12_1$	$P2_12_12_1$	$P2_12_12_1$
Cell dimensions						
a, *b*, *c* (Å)	94.5, 105.2, 118.3	94.3, 103.3, 117.0	94.7, 107.4, 116.9	94.4, 107.0 117.6	89.4, 99.6, 121.4	89.4, 99.6, 121.4
α, *β*, *γ* (°)	90.0, 90.0, 90.0	90.0, 90.0, 90.0	90.0, 90.0, 90.0	90.0, 90.0, 90.0	90.0, 90.0, 90.0	90.0, 90.0, 90.0
Resolution (Å) *	50-3.20 (3.31-3.20)	50-3.40 (3.53-3.40)	50-2.90 (3.00- 2.90)	50-2.55 (2.64-2.55)	50-1.80 (1.86- 1.80)	50-1.85 (1.92-1.85)
R_{merge} *	0.086 (0.57)	0.13 (0.58)	0.14 (0.62)	0.097 (0.60)	0.059 (0.84)	0.052 (0.59)
$I/\sigma I$ *	22.1 (3.0)	12.1 (2.8)	13.1 (3.0)	15.4(2.7)	22.9 (2.5)	23.1 (1.9)
Completeness (%) *	98.4 (99.2)	99.8 (100)	99.8 (100)	99.8 (99.2)	100 (100)	99.2 (99.2)
Redundancy *	6.6 (6.8)	4.4 (4.4)	5.8 (5.9)	6.5 (6.5)	13.3(13.2)	3.7 (3.7)
CC1/2 *	-‡	-‡	-‡	-‡	(0.89)	(0.77)
Refinement						
Resolution (Å)				2.55	1.80	1.85
No. reflections *				39020 (3854)	101068 (10014)	93159 (9182)
R_{work}/R_{free}				0.186, 0.225	0.181, 0.211	0.192, 0.232

Author Manuscript Author Manuscript Author Manuscript Author Manuscript

	Apo-OxsB Native data used for SIRAS	SeMet Apo-OxsB†§ (Se-peak, dataset 1)	SeMet Apo-OxsB†§ (Se-peak, dataset 2)	SeMet Apo-OxsB (Se-peak, dataset 3)	OxsB Cbl/[4Fe4S]	OxsB Cbl/[4Fe4S]/AdoMet
No. atoms						
Protein				5991	5854	6082
Cbl				-	91	91
[4Fe-4S]				-	8	8
AdoMet				-	-	54
DTT				-	8	-
MES				-	12	12
Ethylene glycol				120	120	64
Water				203	664	517
B-factors						
Protein				53.33	37.49	44.66
Cbl				-	29.80	38.93
[4Fe-4S]				-	26.32	31.89
AdoMet//				-	-	A: 40.36 B: 38.29
DTT				-	41.89	-
MES				-	48.20	50.91
Ethylene glycol				61.54	50.68	54.36
Water				53.85	44.99	49.33
R.m.s deviations						
Bond lengths (Å)				0.002	0.010	0.010
Bond angles (°)				0.50	1.176	1.306

*Highest resolution shell is shown in parenthesis

†Bijvoet pairs were not merged during data processing

‡Value was not reported in the version of scalepack used for scaling

§Structure was not refined to completion

//B-factors for two orientations of AdoMet refined at occupancy=0.5 are listed (A=non-radical competent and B=radical competent). When the B-factors are set at 35, the occupancy of each orientation refines to A=0.46 and B=0.54, and when the B-factors are set at 30, the occupancy of each orientation refines to A=0.47 and B=0.53.

Supplementary Material

Refer to Web version on PubMed Central for supplementary material.

Acknowledgments

This work was supported by National Institute of Health Grants F32-GM108189 (J.B.-R.) and GM035906 (H.-w.L.), and the Welch Foundation grant F-1511 (H.-w.L.). C.L.D. is a Howard Hughes Medical Institute Investigator. This work is based upon research conducted at the Northeastern Collaborative Access Team beamlines, which are funded by the National Institute of General Medical Sciences from the National Institutes of Health (P41 GM103403). The Pilatus 6M detector on 24-ID-C beam line is funded by a NIH-ORIP HEI grant (S10 RR029205). This research used resources of the Advanced Photon Source, a U.S. Department of Energy (DOE) Office of Science User Facility operated for the DOE Office of Science by Argonne National Laboratory under Contract No. DE-AC02-06CH11357.

References

1. Shimada N, et al. Oxetanocin, a novel nucleoside from bacteria. J Antibiot (Tokyo). 1986; 39:1623–1625. [PubMed: 3025147]
2. Izuta S, et al. Inhibitory effects of triphosphate derivatives of oxetanocin G and related compounds on eukaryotic and viral DNA polymerases and human immunodeficiency virus reverse transcriptase. J Biochem. 1992; 112:81–87. [PubMed: 1385392]

Author Manuscript Author Manuscript Author Manuscript Author Manuscript

3. Ueda K, Tsurimoto T, Nagahata T, Chisaka O, Matsubara K. An in vitro system for screening anti-hepatitis B virus drugs. Virology. 1989; 169:213–216. [PubMed: 2466368]
4. Morita M, et al. Cloning of oxetanocin A biosynthetic and resistance genes that reside on a plasmid of Bacillus megaterium strain NK84-0128. Biosci Biotechnol Biochem. 1999; 63:563–566. DOI: 10.1271/bbb.63.563 [PubMed: 10227144]
5. Magnusson OT, Reed GH, Frey PA. Characterization of an allylic analogue of the 5′-deoxyadenosyl radical: an intermediate in the reaction of lysine 2,3-aminomutase. Biochemistry. 2001; 40:7773–7782. [PubMed: 11425303]
6. Frey, PA. Liu, L., Mander, H-W., editors. Elsevier; 2010. p. 501-546.
7. Blodgett JA, Zhang JK, Metcalf WW. Molecular cloning, sequence analysis, and heterologous expression of the phosphinothricin tripeptide biosynthetic gene cluster from Streptomyces viridochromogenes DSM 40736. Antimicrob Agents Chemother. 2005; 49:230–240. DOI: 10.1128/AAC.49.1.230-240.2005 [PubMed: 15616300]
8. Kamigiri K, Hidaka T, Imai S, Murakami T, Seto H. Studies on the biosynthesis of bialaphos (SF-1293) 12. C-P bond formation mechanism of bialaphos: discovery of a P-methylation enzyme. J Antibiot (Tokyo). 1992; 45:781–787. [PubMed: 1624380]
9. Kelly WL, Pan L, Li C. Thiostrepton biosynthesis: prototype for a new family of bacteriocins. J Am Chem Soc. 2009; 131:4327–4334. DOI: 10.1021/ja807890a [PubMed: 19265401]
10. Kim HJ, et al. GenK-catalyzed C-6′ methylation in the biosynthesis of gentamicin: isolation and characterization of a cobalamin-dependent radical SAM enzyme. J Am Chem Soc. 2013; 135:8093–8096. DOI: 10.1021/ja312641f [PubMed: 23679096]
11. Liao R, et al. Thiopeptide biosynthesis featuring ribosomally synthesized precursor peptides and conserved posttranslational modifications. Chem Biol. 2009; 16:141–147. DOI: 10.1016/j.chembiol.2009.01.007 [PubMed: 19246004]
12. Marous DR, et al. Consecutive radical S-adenosylmethionine methylations form the ethyl side chain in thienamycin biosynthesis. Proc Natl Acad Sci U S A. 2015; 112:10354–10358. DOI: 10.1073/pnas.1508615112 [PubMed: 26240322]
13. Werner WJ, et al. In vitro phosphinate methylation by PhpK from Kitasatospora phosalacinea. Biochemistry. 2011; 50:8986–8988. DOI: 10.1021/bi201220r [PubMed: 21950770]
14. Westrich L, Heide L, Li SM. CloN6, a novel methyltransferase catalysing the methylation of the pyrrole-2-carboxyl moiety of clorobiocin. Chembiochem. 2003; 4:768–773. DOI: 10.1002/cbic.200300609 [PubMed: 12898629]
15. Woodyer RD, Li G, Zhao H, van der Donk WA. New insight into the mechanism of methyl transfer during the biosynthesis of fosfomycin. Chem Commun (Camb). 2007:359–361. DOI: 10.1039/b614678c [PubMed: 17220970]
16. Sofia HJ, Chen G, Hetzler BG, Reyes-Spindola JF, Miller NE. Radical SAM, a novel protein superfamily linking unresolved steps in familiar biosynthetic pathways with radical mechanisms: functional characterization using new analysis and information visualization methods. Nucleic Acids Res. 2001; 29:1097–1106. [PubMed: 11222759]
17. Allen KD, Wang SC. Initial characterization of Fom3 from Streptomyces wedmorensis: The methyltransferase in fosfomycin biosynthesis. Arch Biochem Biophys. 2014; 543:67–73. DOI: 10.1016/j.abb.2013.12.004 [PubMed: 24370735]
18. Allen KD, Wang SC. Spectroscopic characterization and mechanistic investigation of P-methyl transfer by a radical SAM enzyme from the marine bacterium Shewanella denitrificans OS217. Biochim Biophys Acta. 2014; 1844:2135–2144. DOI: 10.1016/j.bbapap.2014.09.009 [PubMed: 25224746]
19. Blaszczyk AJ, et al. Spectroscopic and Electrochemical Characterization of the Iron-Sulfur and Cobalamin Cofactors of TsrM, an Unusual Radical S-Adenosylmethionine Methylase. J Am Chem Soc. 2016
20. Pierre S, et al. Thiostrepton tryptophan methyltransferase expands the chemistry of radical SAM enzymes. Nat Chem Biol. 2012; 8:957–959. DOI: 10.1038/nchembio.1091 [PubMed: 23064318]
21. Chew AG, Bryant DA. Chlorophyll biosynthesis in bacteria: the origins of structural and functional diversity. Annu Rev Microbiol. 2007; 61:113–129. DOI: 10.1146/annurev.micro.61.080706.093242 [PubMed: 17506685]

Author Manuscript Author Manuscript Author Manuscript Author Manuscript

22. Bridwell-Rabb J, Kang G, Zhong A, Liu HW, Drennan CL. An HD domain phosphohydrolase active site tailored for oxetanocin-A biosynthesis. Proc Natl Acad Sci U S A. 2016; 113:13750–13755. [PubMed: 27849620]
23. Drennan CL, Huang S, Drummond JT, Matthews RG, Ludwig ML. How a protein binds B12: A 3.0 A X-ray structure of B12-binding domains of methionine synthase. Science. 1994; 266:1669–1674. [PubMed: 7992050]
24. Lexa D, Saveant JM. The Electrochemistry of Vitamin-B12. Accounts Chem Res. 1983; 16:235–243. DOI: 10.1021/ar00091a001
25. Vey JL, et al. Structural basis for glycyl radical formation by pyruvate formate-lyase activating enzyme. Proc Natl Acad Sci U S A. 2008; 105:16137–16141. DOI: 10.1073/pnas.0806640105 [PubMed: 18852451]
26. Dowling DP, Vey JL, Croft AK, Drennan CL. Structural diversity in the AdoMet radical enzyme superfamily. Biochim Biophys Acta. 2012; 1824:1178–1195. DOI: 10.1016/j.bbapap.2012.04.006 [PubMed: 22579873]
27. Vey JL, Drennan CL. Structural insights into radical generation by the radical SAM superfamily. Chem Rev. 2011; 111:2487–2506. DOI: 10.1021/cr9002616 [PubMed: 21370834]
28. Goldman PJ, Grove TL, Booker SJ, Drennan CL. X-ray analysis of butirosin biosynthetic enzyme BtrN redefines structural motifs for AdoMet radical chemistry. Proc Natl Acad Sci U S A. 2013; 110:15949–15954. DOI: 10.1073/pnas.1312228110 [PubMed: 24048029]
29. Holm L, Rosenstrom P. Dali server: conservation mapping in 3D. Nucleic Acids Res. 2010; 38:W545–549. DOI: 10.1093/nar/gkq366 [PubMed: 20457744]
30. Bandarian V, Ludwig ML, Matthews RG. Factors modulating conformational equilibria in large modular proteins: a case study with cobalamin-dependent methionine synthase. Proc Natl Acad Sci U S A. 2003; 100:8156–8163. DOI: 10.1073/pnas.1133218100 [PubMed: 12832615]
31. Evans JC, et al. Structures of the N-terminal modules imply large domain motions during catalysis by methionine synthase. Proc Natl Acad Sci U S A. 2004; 101:3729–3736. DOI: 10.1073/pnas.0308082100 [PubMed: 14752199]
32. Koutmos M, Datta S, Pattridge KA, Smith JL, Matthews RG. Insights into the reactivation of cobalamin-dependent methionine synthase. Proc Natl Acad Sci U S A. 2009; 106:18527–18532. DOI: 10.1073/pnas.0906132106 [PubMed: 19846791]
33. Banerjee R. Radical carbon skeleton rearrangements: catalysis by coenzyme B12-dependent mutases. Chem Rev. 2003; 103:2083–2094. DOI: 10.1021/cr0204395 [PubMed: 12797824]
34. Layer G, et al. The substrate radical of Escherichia coli oxygen-independent coproporphyrinogen III oxidase HemN. J Biol Chem. 2006; 281:15727–15734. DOI: 10.1074/jbc.M512628200 [PubMed: 16606627]
35. Ruszczycky MW, Choi SH, Liu HW. Stoichiometry of the redox neutral deamination and oxidative dehydrogenation reactions catalyzed by the radical SAM enzyme DesII. J Am Chem Soc. 2010; 132:2359–2369. DOI: 10.1021/ja909451a [PubMed: 20121093]
36. Shibata N, Masuda J, Morimoto Y, Yasuoka N, Toraya T. Substrate-induced conformational change of a coenzyme B12-dependent enzyme: crystal structure of the substrate-free form of diol dehydratase. Biochemistry. 2002; 41:12607–12617. [PubMed: 12379103]
37. Berkovitch F, Nicolet Y, Wan JT, Jarrett JT, Drennan CL. Crystal structure of biotin synthase, an S-adenosylmethionine-dependent radical enzyme. Science. 2004; 303:76–79. DOI: 10.1126/science.1088493 [PubMed: 14704425]
38. Bradford MM. A rapid and sensitive method for the quantitation of microgram quantities of protein utilizing the principle of protein-dye binding. Anal Biochem. 1976; 72:248–254. [PubMed: 942051]
39. Sambrook, J., Russell, DW. Molecular cloning: a laboratory manual. 3. Cold Spring Harbor Laboratory Press; 2001.
40. Fish WW. Rapid colorimetric micromethod for the quantitation of complexed iron in biological samples. Methods Enzymol. 1988; 158:357–364. [PubMed: 3374387]
41. Stookey LL. Ferrozine - a New Spectrophotometric Reagent for Iron. Analytical Chemistry. 1970; 42:779-&.

Author Manuscript Author Manuscript Author Manuscript Author Manuscript

42. Norbeck DW, Kramer JB. Synthesis of (−)-Oxetanocin. Journal of the American Chemical Society. 1988; 110:7217–7218. DOI: 10.1021/ja00229a048
43. Wu JC, Pathak T, Bazin H, Chattopadhyaya J. Regiospecific synthesis of deuterium-labelled 2′-deoxyribonucleosides. Nucleic Acids Symp Ser. 1987:21–24. [PubMed: 3697131]
44. McCarty RM, Krebs C, Bandarian V. Spectroscopic, steady-state kinetic, and mechanistic characterization of the radical SAM enzyme QueE, which catalyzes a complex cyclization reaction in the biosynthesis of 7-deazapurines. Biochemistry. 2013; 52:188–198. DOI: 10.1021/bi301156w [PubMed: 23194065]
45. Gust B, Challis GL, Fowler K, Kieser T, Chater KF. PCR-targeted Streptomyces gene replacement identifies a protein domain needed for biosynthesis of the sesquiterpene soil odor geosmin. Proc Natl Acad Sci U S A. 2003; 100:1541–1546. DOI: 10.1073/pnas.0337542100 [PubMed: 12563033]
46. Morita M, Tomita K, Sato S, Morino T. Establishment of a host-vector system in Bacillus megaterium strain NK84-0128, an oxetanocin A producer. Bioscience Biotechnology and Biochemistry. 1996; 60:1020–1022.
47. Ewall RX, Bennett LE. Reactivity Characteristics of Cytochrome C(III) Adduced from Its Reduction by Hexaammineruthenium(II) Ion. J Am Chem Soc. 1974; 96:940–942. DOI: 10.1021/ja00810a063
48. Parthasarathy A, et al. Biochemical and EPR-Spectroscopic Investigation into Heterologously Expressed Vinyl Chloride Reductive Dehalogenase (VcrA) from Dehalococcoides mccartyi Strain VS. J Am Chem Soc. 2015; 137:3525–3532. DOI: 10.1021/ja511653d [PubMed: 25686300]
49. Otwinowski Z, Minor W. Processing of X-ray diffraction data collected in oscillation mode. Macromolecular Crystallography, Pt A. 1997; 276:307–326. DOI: 10.1016/S0076-6879(97)76066-X
50. Morin A, et al. Collaboration gets the most out of software. Elife. 2013; 2:e01456. [PubMed: 24040512]
51. Schneider TR, Sheldrick GM. Substructure solution with SHELXD. Acta Crystallogr D Biol Crystallogr. 2002; 58:1772–1779. [PubMed: 12351820]
52. Pape T, Schneider TR. HKL2MAP: a graphical user interface for macromolecular phasing with SHELX programs. Journal of Applied Crystallography. 2004; 37:843–844. DOI: 10.1107/S0021889804018047
53. Vonrhein C, Blanc E, Roversi P, Bricogne G. Automated structure solution with autoSHARP. Methods Mol Biol. 2007; 364:215–230. DOI: 10.1385/1-59745-266-1:215 [PubMed: 17172768]
54. Abrahams JP, Leslie AG. Methods used in the structure determination of bovine mitochondrial F1 ATPase. Acta Crystallogr D Biol Crystallogr. 1996; 52:30–42. DOI: 10.1107/S0907444995008754 [PubMed: 15299723]
55. Emsley P, Cowtan K. Coot: model-building tools for molecular graphics. Acta Crystallogr D Biol Crystallogr. 2004; 60:2126–2132. DOI: 10.1107/S0907444904019158 [PubMed: 15572765]
56. Adams PD, et al. PHENIX: a comprehensive Python-based system for macromolecular structure solution. Acta Crystallogr D Biol Crystallogr. 2010; 66:213–221. DOI: 10.1107/S0907444909052925 [PubMed: 20124702]
57. Moriarty NW, Grosse-Kunstleve RW, Adams PD. electronic Ligand Builder and Optimization Workbench (eLBOW): a tool for ligand coordinate and restraint generation. Acta Crystallographica Section D-Biological Crystallography. 2009; 65:1074–1080. DOI: 10.1107/S0907444909029436
58. Harmer JE, et al. Structures of lipoyl synthase reveal a compact active site for controlling sequential sulfur insertion reactions. Biochem J. 2014; 464:123–133. DOI: 10.1042/BJ20140895 [PubMed: 25100160]
59. Broderick JB, Duffus BR, Duschene KS, Shepard EM. Radical S-adenosylmethionine enzymes. Chem Rev. 2014; 114:4229–4317. DOI: 10.1021/cr4004709 [PubMed: 24476342]
60. Dowling DP, et al. Radical SAM enzyme QueE defines a new minimal core fold and metal-dependent mechanism. Nat Chem Biol. 2014; 10:106–112. DOI: 10.1038/nchembio.1426 [PubMed: 24362703]

Author Manuscript Author Manuscript Author Manuscript Author Manuscript

61. Layer G, et al. The substrate radical of Escherichia coli oxygen-independent coproporphyrinogen III oxidase HemN. J Biol Chem. 2006; 281:15727–15734. DOI: 10.1074/jbc.M512628200 [PubMed: 16606627]

62. Nicolet Y, Amara P, Mouesca JM, Fontecilla-Camps JC. Unexpected electron transfer mechanism upon AdoMet cleavage in radical SAM proteins. Proc Natl Acad Sci U S A. 2009; 106:14867–14871. DOI: 10.1073/pnas.0904385106 [PubMed: 19706452]

63. Quitterer F, List A, Eisenreich W, Bacher A, Groll M. Crystal Structure of Methylornithine Synthase (PylB): Insights into the Pyrrolysine Biosynthesis. Angew Chem Int Edit. 2012; 51:1339–1342. DOI: 10.1002/anie.201106765

64. Goldman PJ, et al. X-ray structure of an AdoMet radical activase reveals an anaerobic solution for formylglycine posttranslational modification. Proc Natl Acad Sci U S A. 2013; 110:8519–8524. DOI: 10.1073/pnas.1302417110 [PubMed: 23650368]

Author Manuscript Author Manuscript Author Manuscript Author Manuscript

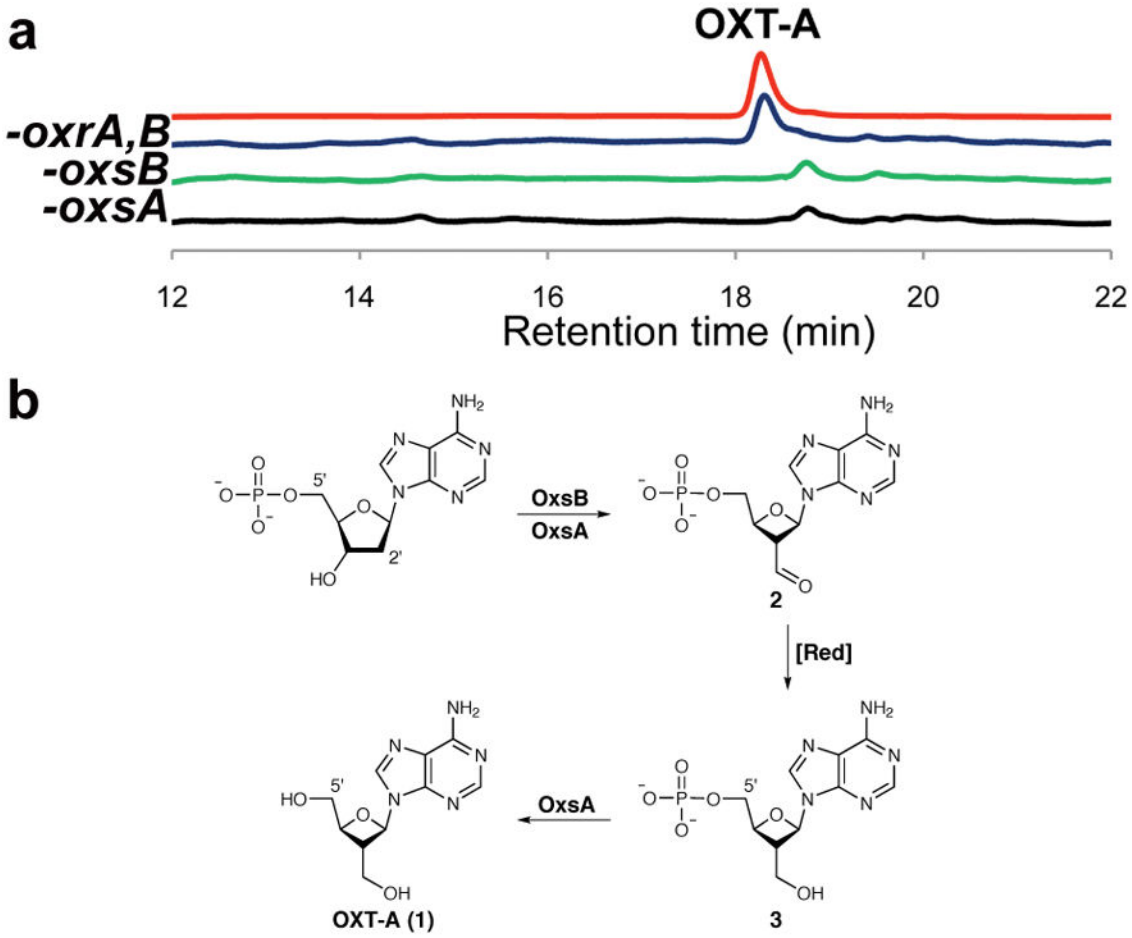

Figure 1.

oxsA and *oxsB* encode OXT-A biosynthetic enzymes. **(a)** In vivo product profiles of *B. megaterium* NRS 269 strains with the designated genes deleted. The top trace is an OXT-A standard. **(b)** Proposed pathway for OXT-A biosynthesis, which requires OxsA, OxsB, and aldehyde reduction to go to completion.

Author Manuscript Author Manuscript Author Manuscript Author Manuscript

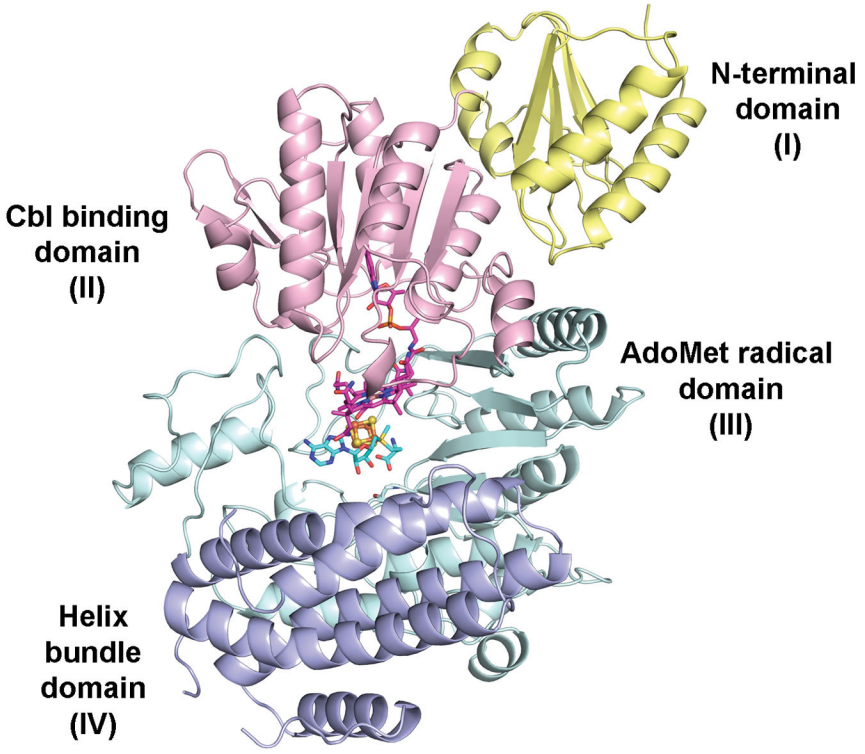

Figure 2.

Structure of OxsB. The monomer contains four domains: an N-terminal domain of unknown function (domain I, yellow), a Rossmann fold that houses Cbl (domain II, pink), a partial triose phosphate isomerase barrel AdoMet radical domain (domain III, cyan), and a C-terminal helix bundle (domain IV, blue). See also Extended Data Fig. 6. Cbl in pink, AdoMet in cyan, [4Fe-4S] cluster in orange/yellow.

Author Manuscript Author Manuscript Author Manuscript Author Manuscript

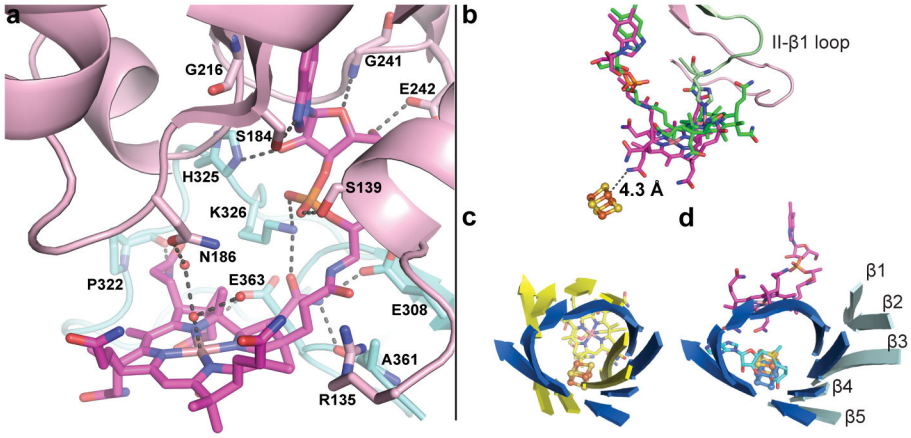

Figure 3.

A new mode of Cbl binding. **(a)** Cbl (pink) interacts with residues in the OxsB Cbl-binding (pink) and AdoMet radical (cyan) domains. **(b)** Cbl in MetH (green) and OxsB (pink) have different positions. The OxsB AdoMet radical [4Fe-4S] cluster is shown as spheres. **(c)** Cbl-dependent diol dehydratase[36] (yellow) and AdoMet radical enzyme biotin synthase[37] (blue) position cofactors at the C-terminal ends of barrels. **(d)** An overlay of the TIM barrel β-strands of OxsB with biotin synthase places the [4Fe-4S] clusters in similar postions and showcases a new Cbl position.

Author Manuscript Author Manuscript Author Manuscript Author Manuscript

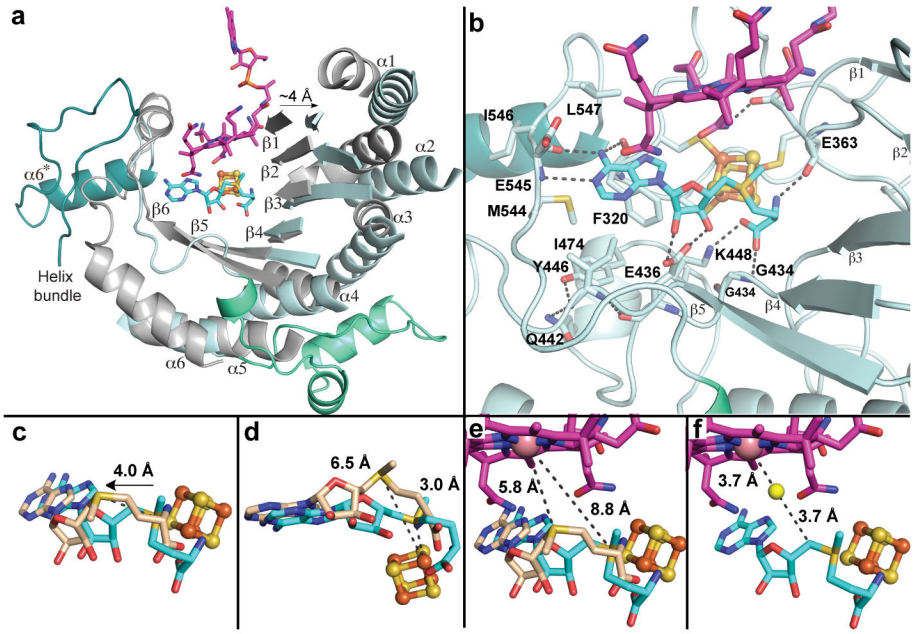

Figure 4.

An expanded AdoMet radical domain in OxsB. **(a)** Comparison of OxsB (cyan) and PFL-AE[25] (gray) reveals OxsB has has additional α-helices ($\alpha 6_a$, $\alpha 6_b$, 3_{10}, α6*) and a more open barrel due to displacement of III-β1, III-α1, III-β2, and III-α2. **(b)** AdoMet binding motifs are conserved in OxsB. Also see Extended Data Fig. 9a. **(c)** AdoMet binds to OxsB in two orientations. **(d)** One AdoMet orientation is not poised for electron transfer (wheat), whereas the other conformation appears radical-competent (cyan). **(e)** The non-radical-competent orientation places the methyl group close to Co. **(f)** The putative substrate-binding site of OxsB (yellow).

Author Manuscript Author Manuscript Author Manuscript Author Manuscript

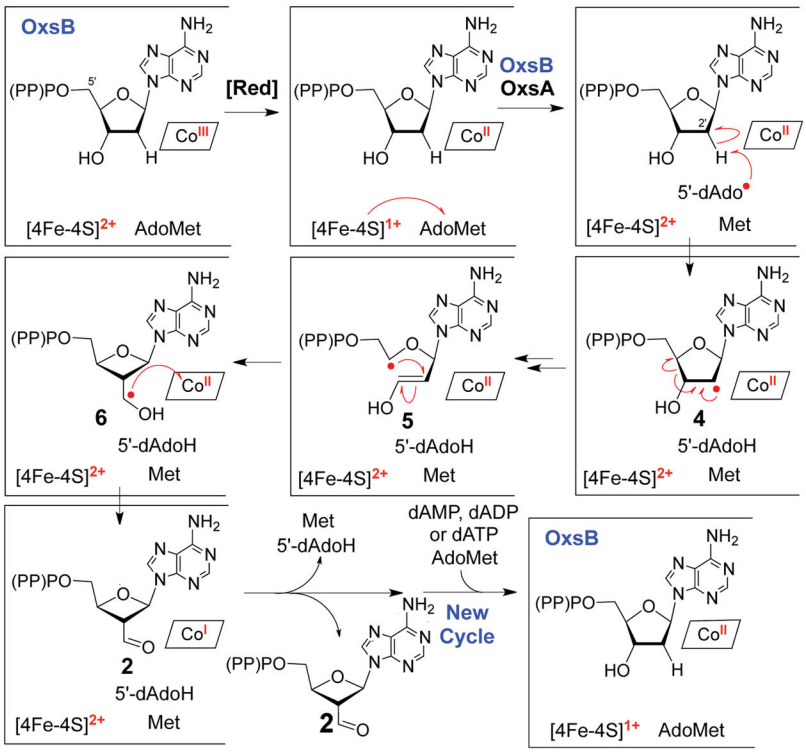

Figure 5.
Mechanistic proposal for generation of OXT-A aldehyde **2**.